



Numerical simulations of free roll decay of DTMB 5415

Metin Kemal Gokce^{a,c}, Omer Kemal Kinaci^{b,*}

^a Naval Architecture and Maritime Faculty, Yildiz Technical University, Turkey

^b Faculty of Naval Architecture and Ocean Engineering, Istanbul Technical University, Turkey

^c Ceyhan Engineering Faculty, Cukurova University, Turkey

ARTICLE INFO

Keywords:

Ship roll
DTMB 5512
Wave damping
Viscous damping
Forward speed effect

ABSTRACT

Computational fluid dynamics (CFD) that implement finite volume method are offering accurate and precise solutions for ship roll problem. In this study, the free roll decay of the benchmark DTMB 5415 hull with bilge keels in calm water was numerically solved by applying this type of code. Contributions of viscosity, wave, eddy and forward ship speed were separately investigated for ship roll damping and these were integral part of experimental setups. Numerical results were first validated with experiments. Additionally, mathematical derivations of ship roll response were used where experiments were impractical or inapplicable. Related literature still lacks a validation procedure. Therefore, a detailed analysis was made for the numerical estimation of roll damping. The weaknesses of CFD and the mathematical model were identified and discussed by comparing the obtained results. The results indicated that although the numerical simulations successfully captured the decay coefficients, these simulations lacked accuracy in calculating the natural roll frequency.

1. Introduction

Computational fluid dynamics (CFD) approach involving the solution of Reynolds-Averaged Navier Stokes Equation (RANSE) for solving ship motions is a popular method to assess the hydrodynamic performance of ships. Although potential theory-based methods are still widely used, viscous effects involving turbulence is excluded from these methods. Viscosity can only be incorporated if the flow is laminar by using Falkner-Skan Equations which can be derived using the Navier-Stokes Equations. Efforts to include turbulent flow effects were inadequate to fully model the characteristics of the flow and therefore were failed to be adopted extensively.

While the ship roll motions are mainly predicted with decades-old methods, these are coupled with empirical estimations of viscous forces to reinforce the calculation procedures. Viscosity has significant effects on roll motion of a ship and all approaches that neglect viscous forces in roll is considered insufficient (Himeno, 1981). Estimation model of Ikeda (Ikeda et al., 1978) is a fast and practical method to solve the roll damping of ships which heavily relies on empirical data obtained from excessive number of experiments. Researches of Ikeda included viscosity in terms of skin friction damping in addition to the remaining four components namely; eddy, wave, lift and bilge keel damping. Method proposed by Ikeda is still widely adopted by many researchers in this

field. However, his empirical method is ineffective in various cases including shallow draft (Yildiz et al., 2016). Such restrictions and shortages in this semi-empirical approach led researchers to utilize the fully nonlinear RANSE based methods that are flexible to generate results in wider scope. An overview regarding ship roll prediction methods is given in (Falzarano et al., 2015).

As FVM has reached the current state, in last two decades, the number of RANSE-based studies for solving ship roll motion have increased. High speed computers led the way for using higher number of elements and enabled implementation of more flexible grid techniques for simulation of ship roll which included the overset (or chimera) grids. Overset grids have found wide application opportunities in numerically simulating ship roll among many researchers working in this field such as (Chen and Liu, 2002), (Araki et al., 2014), (Sadat-Hosseini et al., 2016) and (Begovic et al., 2017a,b). These researchers have implemented this specific type of dynamic mesh system. These types are especially beneficial for simulating large ship roll angles.

Ship roll is one of the most poorly understood ship motions as discussed by (Falzarano et al., 2015). Therefore, this method is appealing to researchers in computational sciences. As the numbers of studies regarding computationally approach the ship roll problem has increased, there are various experimental studies especially published for providing data for CFD simulations. (Lee et al., 2012) and (Lee et al., 2016) have

* Corresponding author.

E-mail address: kinacio@itu.edu.tr (O.K. Kinaci).

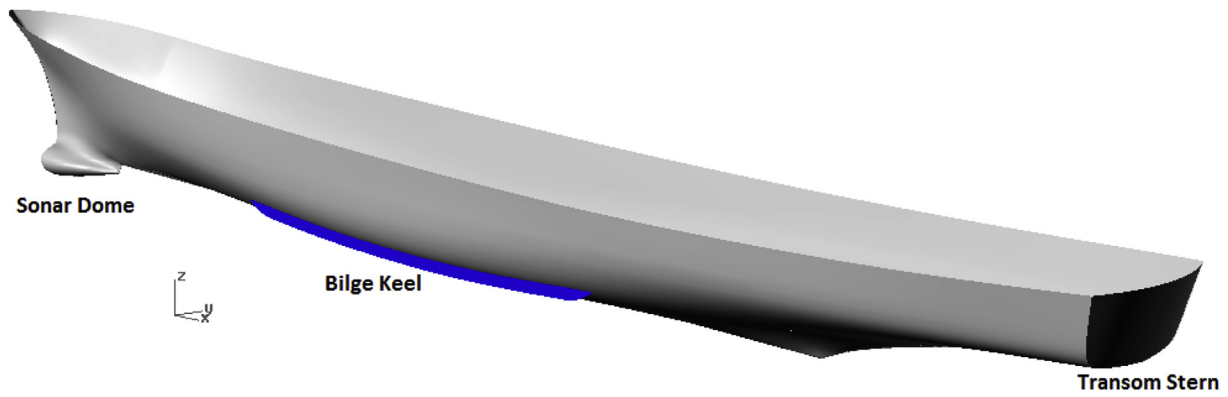


Fig. 1. A perspective view of the DTMB model 5512.

published experimental data to develop better CFD methods. ITTC have published a guideline for numerical estimation of roll damping for these CFD studies to comply with (ITTC 7.5-02-07-04.5, 2011). Although previous studies addressed ship roll response for intact condition only, roll response in damaged condition is also analyzed in recent studies (Gao and Vassalos, 2011; Lee et al., 2012; Begovic et al., 2017a,b; Sadat-Hosseini et al., 2016; Acanfora and De Luca, 2016; Begovic et al., 2017a,b).

This study focused on free roll decay of a benchmark ship DTMB 5415 implementing a RANSE based CFD approach. Numerical solution of roll motion using RANSE based CFD is still relatively an unexplored section of ship hydrodynamics. Although the interest towards numerical simulations have increased recently, similar studies are rarely found in the literature. In some studies, such as (Irkal et al., 2016), reported that there is still a shortage in CFD simulations of free roll decay of ships. It is believed that more numerical results are needed to establish a general approach to the problem.

One of the purposes of this study was to identify the contributions of wave and eddy damping, viscous damping and the effect of forward speed on ship roll motion. To evaluate the effect of each component, inviscid solver as well as the analytical approach was adapted. Such an approach, which only covered viscous and eddy damping only by mirroring the geometry in the water-plane and solving it with a double body, was previously adopted by (Jaouen et al., 2011). The flexibility of commercial software (in this study, Star CCM+ was used and the details of the numerical approach were given and explained in the following chapters) implementing RANSE also contributed to simplify the problem and to obtain faster results. Roll damping was assessed by making a free roll decay numerical simulation. Wasserman et al. (2016) stated that free roll decay has certain advantages over harmonic excited roll motion technique while roll damping was estimated. The authors stated that it is especially beneficial when there is no forward ship speed and damping are small.

Analytical solutions to uncoupled roll motion of ships are mentioned where applicable. In this study, the analytical solution (presented in

Section 5 as a second order ordinary differential function) was adopted for understanding the *theoretically mandatory motion of the ship hull under inviscid/viscous flow and calm free water surface conditions with zero forward hull speed*. This approach was selected as a reference to assess the CFD based results; although there are certain drawbacks of this evaluation procedure. First, the analytical solution includes the hull form effects in a very limited manner due to linearized approach. Secondly, the CFD based results are always prone to errors such as numerical errors, modeling errors etc. Thus, these results must be evaluated carefully. Both methods have certain advantages and certain disadvantages. Thus, the limitations of these methods should be discovered to use them effectively.

2. Geometric and hydrostatic properties of DTMB model 5415

Numerical roll decay simulations were made for the DTMB 5512 hull, where various experimental and numerical results are available in the literature. The DTMB 5512 is a geosim of the full scale DTMB 5415 ship at 1/46.6 model scale. The hull contains a sonar dome, bilge keels on both sides of the ship and has a transom stern. The geometry of DTMB 5512 is shown in Fig. 1.

The propulsion is provided through twin propellers and the ship has twin rudders which are excluded in Fig. 1. These appendages were excluded in roll decay CFD simulations. In this study, bilge keel was considered as appendage in numerical simulations. Effect of bilge keels on roll damping was investigated by many studies in the field such as (Irvine et al., 2013; Araki et al., 2014; Avalos et al., 2014; Irkal et al., 2014, 2016); therefore, the bilge keel effect was not separated as a stand-alone case. The hydrostatic and geometric properties of the DTMB model 5512, including the bilge keel, are given in Table 1. When values given in the Table were considered, it is important to note that the origin (0, 0) is set where the bow meets the waterline.

Table 1

Hydrostatic properties of the DTMB hull model 5512; a geosim of DTMB 5415 at model scale.

Parameter	Symbol	Unit	Model 5512
Length	L	m	3.048
Beam	B	m	0.405
Draft	T	m	0.132
Wetted surface area	S_w	m^2	1.459
Block coefficient	C_B	–	0.506
Metacentric height	GM	m	0.043
Longitudinal center of gravity	LCG	m	1.536
Vertical center of gravity	VCG	m	0.030
Roll radius of gyration	k_ϕ	m	0.158
Natural roll period	T	s	1.54

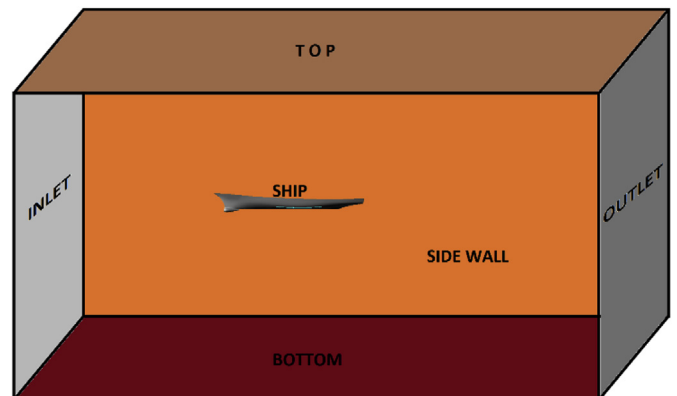


Fig. 2. Boundaries of the numerical simulations.

Table 2
Boundary conditions.

BOUNDARY	CONDITION
Inlet	Velocity inlet
Outlet	Pressure outlet
Top	No slip, stationary wall
Bottom	No slip, stationary wall
Side walls	No slip, stationary wall
Ship	No slip, stationary wall

3. Numerical approach

3.1. Numerical simulation conditions

All the simulations in this study were either uncoupled roll motions or only coupled with the surge motion of the ship. Surge was included in the numerical simulations to assess the effect of forward speed on ship roll. In this respect, the numerical simulations either had one degree-of-freedom (1-DOF) or 2-DOF. The fluid domain boundaries and the boundary conditions are given in Fig. 2 and Table 2 respectively. Domain extents were selected in line with the recommendations of the (ITTC 7.5-03-02-03, 2011). Fig. 2 is unscaled.

3.2. Grid structure

Hexahedral elements were used, to solve the flow around hull for the implemented grid structure. The hull was released to roll decay and

during the simulations, elements in the fluid domain were deformed with respect to the motion. This was realized using the morphing grid option available in Star CCM + software. A general view of the elements can be seen in Fig. 3. This type of grid system deforms the elements in the vicinity of the hull during roll decay by reconstructing the boundaries with respect to the movement of the control points. In this study, the control points were selected from the boundaries of the element and the displacements of the control points were calculated by an interpolation field in the region.

Morphing (or deforming) grid was considered as a good selection for small ship motions. Other possible options such as overset grid or rigid body motion would have disadvantages in simulating ship roll. For example, in rigid body motion, the fluid domain would be rotated instead of the ship itself which leads to problems with accurate prediction of the free surface. Overset grid, on the other hand, needs large computer memory due to high number of element requirement (Sukas et al., 2017). High computational cost reduces the applicability of the overset grid option. Although morphing grid could be a suitable option for this study, it would be disadvantageous for ships rolling in large angles. Elements deforming with respect to the ship would get skew in large motions which might lead to generation of nonphysical results. While small roll angles adopted in this study were considered, no additional adjustments in the morpher solver were made and the commercial software was used with default settings.

This type of grid structure has three important zones. The first one is the Kelvin waves zone which is marked as (1) in the Figure. This zone allows better simulation of the wake (especially during surge which is

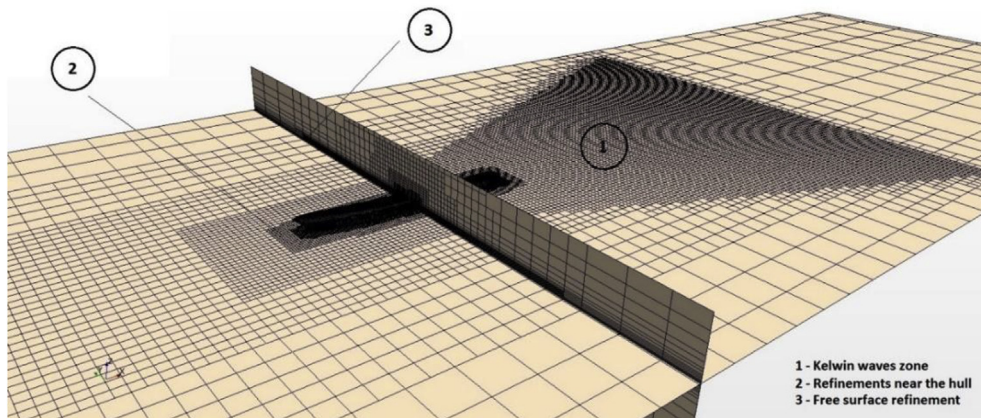


Fig. 3. Grid structure implemented in the fluid domain for roll decay numerical simulations.

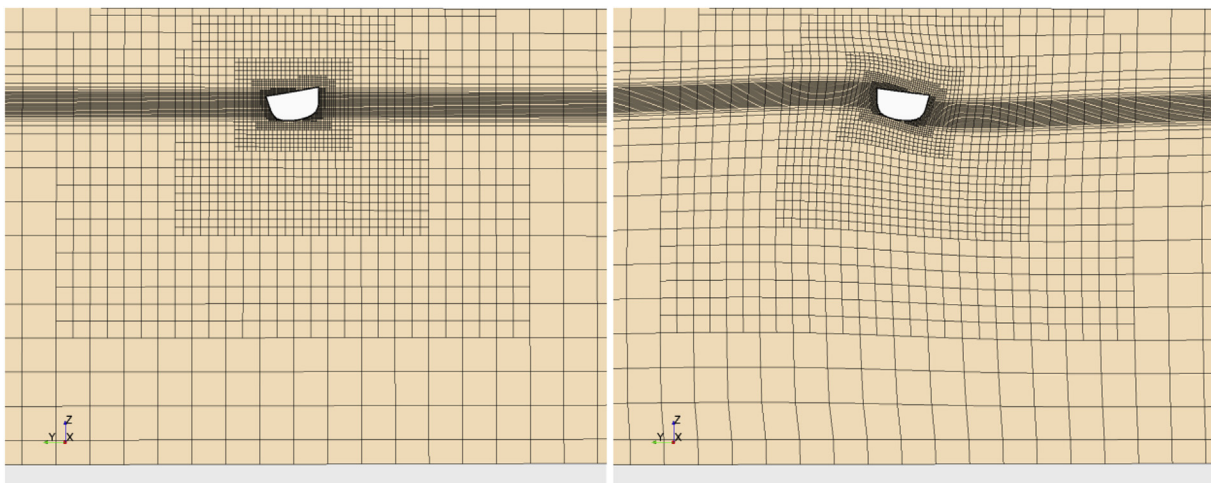


Fig. 4. Initial grid structure at $t = 0$ (left). Deformed grid structure at $t = T/2$ (right).

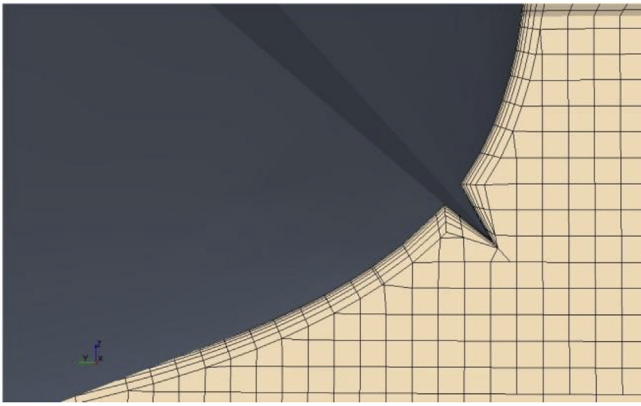


Fig. 5. The prism layer around the bilge keel.

available for cases when $Fr > 0$). The refinement is generally on xy plane with a small thickness along z direction that is expected to cover the free surface deformations. The second zone covers the refinements near the hull which is marked as (2) in Fig. 3. This zone is a block that surrounds the hull. The elements near the boundaries of the ship were selected small to capture correctly the flow characteristics during the roll motion. The free surface refinement marked as (3) in the same Figure is only in z direction and this is to ensure that the deformations in the water surface are correctly represented.

The morphing motion in the software calculates the new coordinates of the elements at each time step. As the hull rolls from one side to the other, the fluid in the rolled side is deferred. This displaced fluid is represented by deforming elements and the displacement of each element is calculated by the induced velocities. The initial grid along yz plane in the fluid domain (when $\phi = \phi_0$ at $t = 0$) is given in Fig. 4 (left) and the deformed grid (when $\phi = -\phi_1$ at $t = T/2$) in the same plane is given in Fig. 4 (right). Morphing grid structure may pose problems for the elements in the fluid domain when there are large translations or rotations of the structure. The roll amplitude in this study was chosen relatively small ($\phi_0 = 10^\circ$) to prevent skew elements being formed especially around the hull. (Araki et al., 2014) have also implemented morphing grid for small roll angles. The authors have used morphing grid along with the overset grid. The fluid domain of that study consisted of an overlapping grid that surrounded the rolling hull and that overlapping grid was surrounded by a morphing grid. The study ensured that no skew elements were formed by selecting close morphing area. For details, refer to (Araki et al., 2014).

Smaller elements, especially near the bilge keels, provide accurate simulation of the flow field and captures vortices formed at this part of the ship. There were 6 prism layers around the hull to approximate the flow in the vicinity of the hull more accurately. The prism layer was fixed and was not subjected to any deformations. The grid structure around the bilge keel is given in Fig. 5.

3.3. Numerical modeling

In this study, Star CCM + commercial software was adopted for simulations. The flow was assumed incompressible and the momentum equations in tensor form using Cartesian coordinate system can be given as:

$$\frac{\partial(\rho \bar{u}_i)}{\partial x_i} = 0$$

$$\frac{\partial(\rho \bar{u}_i)}{\partial t} + \frac{\partial}{\partial x_j} (\rho \bar{u}_i \bar{u}_j + \rho \overline{u_i' u_j'}) = -\frac{\partial \bar{p}}{\partial x_i} + \frac{\partial \bar{\tau}_{ij}}{\partial x_j} + \rho f_i$$

where $\bar{\tau}_{ij} = \mu \left(\frac{\partial \bar{u}_i}{\partial x_j} + \frac{\partial \bar{u}_j}{\partial x_i} \right)$ are the mean viscous stress tensor component, \bar{p}

the mean pressure, \bar{u}_i is the averaged Cartesian components of the velocity vector, $\rho \overline{u_i' u_j'}$ the Reynolds stresses. ρ denotes the density of the fluid and μ is the dynamic viscosity. f_i is the body force where it is only defined by gravitational acceleration in the z direction as $f_3 = -g$ and present in the RANS solver due to the two-phase flow around the ship.

URANS equations along with $k - \epsilon$ turbulence model were solved in an implicit unsteady solver. $k - \omega$ SST model was also experienced if the selection of the turbulence model had any effects on free roll decay. There were no significant distinctions between the findings of this study and of (Begovic et al., 2017a,b). Free surface effects that account for the wave damping of the roll motion were modeled with Volume of Fluid (VOF) method. To correctly model the wave deformations close to the ship, grid refinements were made close to the free surface (see Fig. 3). The refinements were made especially in the z direction so that there would be a better prediction of the interface between the air and water phases. In the VOF method, the free surface is indicated by a fraction that represents the water-air interface. Water phase fraction was given as 1, air phase as 0, and water-air interface, that is the free surface in this study, was denoted by 0.5. The side wall boundary condition was selected as “velocity inlet” to prevent wave reflection from the sides during the roll motion. The dynamic fluid-body interaction model (DFBI) was activated in the software to solve for time-dependent motion. Due to the nature of moving bodies inside the fluid, dynamic mesh system is required for numerical approach of the problem. Morphing grid option (details of this options was explained in the previous section), that allows deformations of the elements in the fluid domain, was selected in the software. If the initial roll angle was large; for the risk of generation of skew elements, grid deformations can be problematic. However, this option was especially selected among the other dynamic mesh system alternatives (such as rigid or overset grid systems) due to easy implementation and robust stability.

The time step size was selected according to the ITTC CFD guidelines (ITTC 7.5-03-02-03, 2011). In the guideline, it is advised that for periodic phenomena such as roll decay, at least 100-time steps shall be used. To adopt a safe operation, one period of roll decay was divided roughly into 150-time steps which resulted in a time step size of $\Delta t = 0.01s$. Inner iteration number was set to 10. This value was considered sufficient to obtain lower residuals and more accurate simulations. To restrain y^+ values on the hull and to keep these values at desired levels; the maximum boundary layer thickness of a flat plate (whose length is equal to the length of the hull) was calculated and used as a reference while the base sizes of the elements on the hull were specified. Hull forms have round bodies and the boundary layer thickness on the hull surface would be different on flat plate. However, this quick calculation gives a rough idea on how many elements were to be expected in the fluid domain. This situation is useful before instantly starting to generate the grid structure.

Although ITTC recommendations stated dividing the periodic phenomena such as roll to at least 100-time steps; Begovic et al. (2017a,b) recommended reducing the time step one order lower. The authors stated that numerical simulations performed better with lower time step sizes and found that roll periods were improved. To test the simulation results in this study, another numerical simulation was applied for roll decay with a time step size of $\Delta t = 0.001s$. This time step value is ten times smaller than ITTCs recommendations. It was found that the results hardly changed with smaller time step sizes as the difference in the roll period was only 0.15%. As such small changes and extra computational operations were considered, for all numerical calculations in this study, time step size of $\Delta t = 0.01s$ was selected. By means of the discrepancy in selecting Δt , there is a contradiction between Begovic et al. (2017a,b) and our numerical simulations. The underlying reason of this contradiction might be caused by the CFL condition. As known, CFL condition is related with the selected time step size and the distance of the first cell from the boundaries. However, Begovic et al. (2017a,b) was unable to provide any

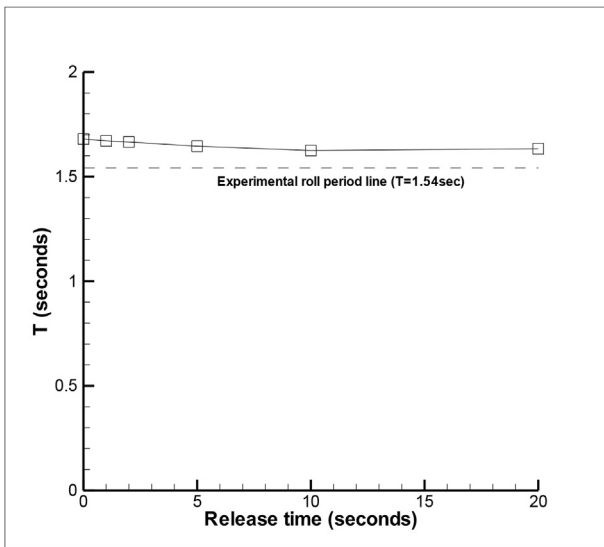


Fig. 6. Numerically obtained roll period versus release time in CFD.

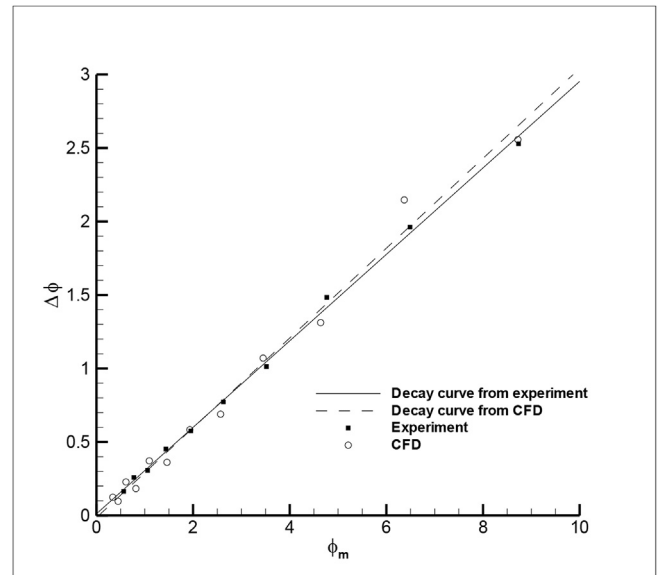


Fig. 8. Curve of decay graphs calculated from roll angle histories given in Fig. 7.

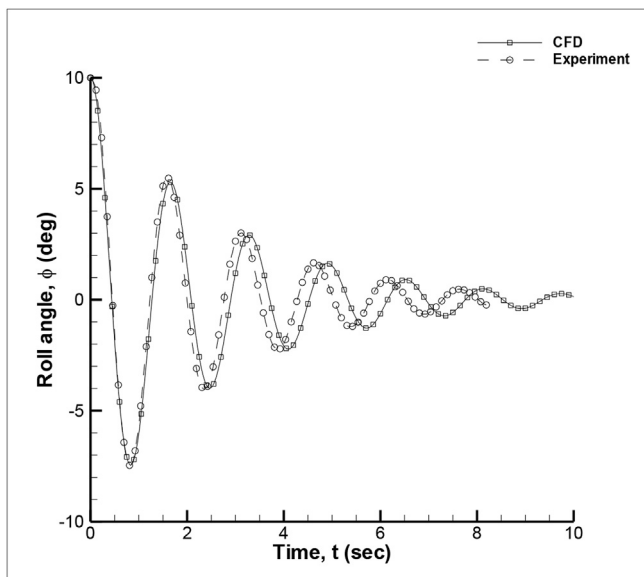


Fig. 7. Free roll decay with an initial angle $\phi_0 = 10^\circ$ at $Fr = 0.41$.

details about the distance of the first cell from the ship's boundaries. Therefore, it is impossible to continue research on the selection of the time step size. On the other hand, our results indicated that the results were independent of the time step size. This meant that the CFL condition was satisfied.

3.4. Importance of 'release time' in roll decay CFD simulations

Similar to usual practices deployed in experiments, at the beginning of CFD simulations, initial roll angle was given to the ship. However, the iterative nature of numerical simulations causes the wave system around the hull to be established late. This drawback of the CFD simulations was covered by the "release time" option that is available in some CFD commercial software. During this "release time", the ship hull was held stationary at the initial roll angle provided by the user and no ship motions were allowed. The code uses this time to solve for the waves generated at the free surface that instantly occurs in experiments. After the settlement of the wave system around the hull (which is expected to

be visible at the end of the release time), the ship motion was allowed.

The default value of release time in Star CCM+ is 1 s. Yet, this usually is insufficient to create waves generated by the ship at the given speed. To completely establish the expected wave system in the fluid domain for roll decay simulations, setting release time to 6–8 s is advised. It should be noted that this value is not scientifically quantified. However, this value purely depends on observation and experience. Roll periods with respect to various release times are given in Fig. 6.

Fig. 6 indicates that the roll periods converge at around $T = 1.62$ s. Before any roll motion of the ship, 10 s release time was between acceptable limits to establish flow system around hull. Therefore, in this study, 10 s of release time was adopted in all numerical simulations.

4. Experimental validation

The validation of the numerical procedure adopted in this study was made with the experimental results of (Irvine et al., 2013). The hull was set free to roll decay with an initial roll angle of $\phi_0 = 10^\circ$ and with a forward velocity at $Fr = 0.41$. The comparison of numerical results of this study and experiments of (Irvine et al., 2013) are given in Fig. 7.

In (ITTC 7.5-02-07-04.5, 2011), there is no suggestion regarding any uncertainty analysis method in the recommended procedure. In this study, CFD validation was obtained in two steps which are specific to numerical estimation of roll damping. Compliance with experiments was sought in terms of the agreement of the decay (and extinction) coefficients and the natural roll period. The decay coefficients constitute the vertical agreement of the graph given in Fig. 7 as the natural roll period composes the horizontal agreement. A grid dependency study was also carried out and provided at the end of this section.

4.1. Validation with the decay and extinction coefficients

The peaks of the roll angle given in Fig. 7 seems compatible in both methods which indicate a vertical agreement of CFD. (ITTC 7.5-02-07-04.5, 2011) recommended that the decay curve should be fit into a third-degree polynomial. In this section, the decay and extinction coefficients for roll decay at $Fr = 0.41$ were calculated. The peaks of the roll graph in Fig. 7 are listed in Table 3 and the coefficients are listed in Table 4.

Using the relations;

Table 3
Numerical and experimental peaks of the roll response given in Fig. 7.

CFD	<i>i</i>	0	1	2	3	4	5	6	7	8	9	10	11	12
	ϕ_i (deg)	10	7.44	5.50	3.98	2.91	2.22	1.64	1.28	0.91	0.72	0.50	0.40	0.28
	<i>t</i> (s)	0	0.83	1.66	2.47	3.28	4.09	4.9	5.72	6.52	7.32	8.12	8.92	9.73
	ϕ_m (deg)	8.72	6.47	4.74	3.45	2.57	1.93	1.46	1.09	0.82	0.61	0.45	0.34	–
	$\Delta\phi$	2.56	1.95	1.51	1.07	0.69	0.58	0.36	0.37	0.18	0.23	0.10	0.12	–
EXPERIMENT	<i>i</i>	0	1	2	3	4	5	6	7	8	9	10	11	12
	ϕ_i (deg)	10	7.47	5.51	4.03	3.01	2.24	1.66	1.21	0.91	0.65	0.48	0.48	0.48
	<i>t</i> (s)	0	0.82	1.59	2.35	3.13	3.89	4.64	5.40	6.10	6.95	7.65	8.35	9.05
	ϕ_m (deg)	8.74	6.49	4.77	3.52	2.63	1.95	1.44	1.06	0.78	0.56	–	–	–
	$\Delta\phi$	2.53	1.96	1.48	1.01	0.77	0.58	0.45	0.31	0.26	0.16	–	–	–

The equations of the decay curve were $\Delta\phi = -0.0019\phi_m^3 + 0.0216\phi_m^2 + 0.2428\phi_m$ numerically and $\Delta\phi = -0.0017\phi_m^3 + 0.0202\phi_m^2 + 0.2363\phi_m$ experimentally As shown in Table 4, generated decay and extinction coefficients are given. These equations are shown in Fig. 8.

Table 4
Decay and extinction coefficients calculated numerically and experimentally.

Coefficients	<i>a</i>	<i>b</i>	<i>c</i>	α	β	γ
CFD	0.2428	0.0216	-0.0019	0.2994	0.9282	-1.3665
Experiment	0.2363	0.0202	-0.0017	0.3092	0.8680	-1.1524

$$T_{n,s} = T_{n,m} \cdot \sqrt{\lambda}, \quad \omega_{n,s} = \omega_{n,m} / \sqrt{\lambda}, \quad \alpha_s = \alpha_m / \sqrt{\lambda}, \quad \beta_s = \beta_m, \quad \gamma_s = \gamma_m \cdot \sqrt{\lambda}$$

where the subscripts *s* and *m* denote ship and model scales respectively. Comparison between the experimental and numerical results are given in Table 5.

Table 5
Computational and experimental results for roll period, frequency and extinction coefficients.

	Model scale					Full scale				
	α_m	β_m	γ_m	$\omega_{n,m}$	$T_{n,m}$	α_s	β_s	γ_s	$\omega_{n,s}$	$T_{n,s}$
CFD	0.2994	0.9282	-1.3665	3.8745	1.6217	0.0439	0.9282	-9.3283	0.5676	11.0702
Experiment	0.3092	0.8680	-1.1524	4.1107	1.5285	0.0453	0.8680	-7.8668	0.6022	10.4341

Table 6
Maximum peaks of the roll angle given in Fig. 13.

<i>t</i> (s)	1.66	3.33	4.98	6.61	8.25	9.87	11.49	13.13	14.75	16.37	18.00	19.61	21.23	22.85	24.45
ϕ (deg)	8.51	7.10	6.08	5.68	5.33	4.86	4.49	4.09	3.58	3.39	3.29	3.13	2.95	2.76	2.71

4.2. Validation with the natural roll period

The natural roll periods given by numerical simulations are given in Fig. 7. These should also be compatible with the experiments. This compatibility reveals the horizontal compliance of the roll decay history. Fig. 7 shows that the horizontal compliance of numerical simulations with the experiments was below the vertical compliance of the roll history curve levels. For the assessment of the numerical validation, natural roll periods should be calculated.

Using the hydrostatic properties of the ship given in Table 1, the undamped roll period was calculated as $T = 1.5285s$. In their study, (Irvine et al., 2013) found the roll period as $T = 1.54s$. This difference was caused by the damping factors such as viscosity, waves etc. The natural roll period calculated from the numerical simulations in this

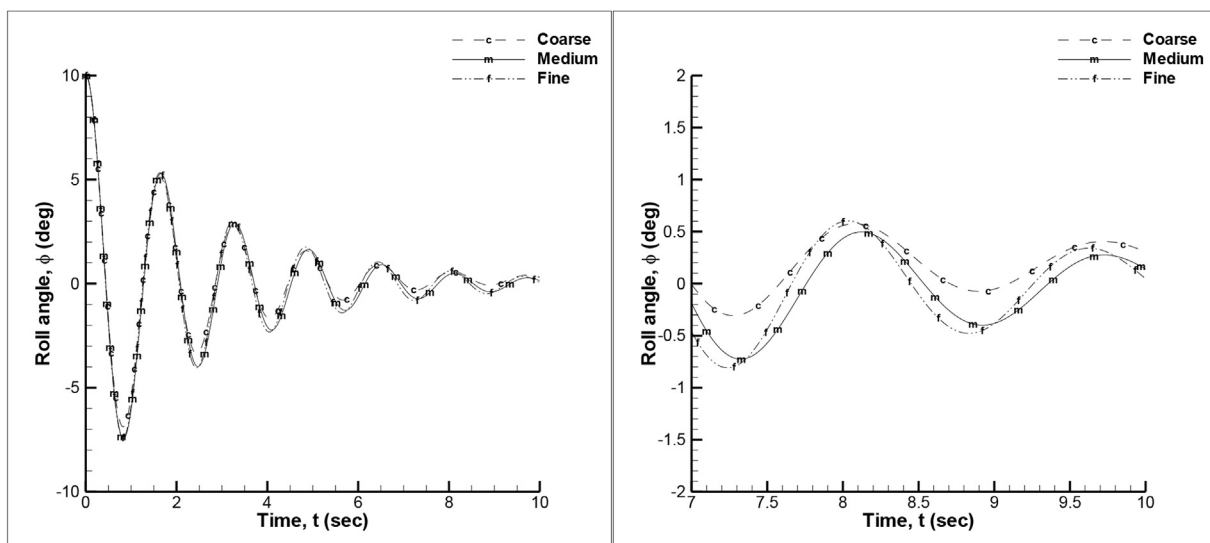


Fig. 9. Numerical roll response using different number of elements. First 10 s (left). A closer view of the last 3 s (right).

study suggested a mean roll period of $T = 1.62s$, which pointed around 5% difference with the experiments. The difference in roll history given in Fig. 7 is further mentioned at the later stages of the motion. This is linked with addition of the miscalculation of the roll period in CFD simulations at each cycle.

It was observed that the natural roll periods were relatively higher than expected values. It should be noted that this was observed in various studies (Gao et al., 2011; Avalos et al., 2014; Irkal et al., 2016) as well as this study. In all these studies, vertical compliance of roll decay history was successfully achieved. However, the horizontal compliance which constitutes the roll decay period has lower achievement ratios. One counter example to this situation was the study of (Araki et al., 2014) where the authors used overset and morphing grids together. In their study, the horizontal agreement was better than the vertical agreement in roll decay. Another study implementing the overset mesh was (Gu et al., 2016). They obtained a good match with the experiments for natural roll period. Yet, they also stated that roll amplitudes were slightly over-predicted. They have also tried using sliding mesh, but the results were lower than overset mesh results. Regarding these flaws of numerical simulations, 5% difference obtained between the experiments was considered acceptable.

4.3. Grid dependency

With increasing number of grid elements in the fluid domain, grid dependency study was conducted for $\lambda = 0.41$. The ship was released to roll decay with an initial roll angle of $\phi_0 = 10^\circ$ using 450k (coarse grid), 1M (medium grid) and 2.2M elements (fine grid). While increasing the number of elements in the fluid domain, element sizes in all directions were reduced isotropically except the Kelvin waves zone refinement and the free surface refinement (see Fig. 3). The element sizes were anisotropic in the x and y directions for the Kelvin waves zone refinement and in the z direction for the free surface refinement. The results are depicted in Fig. 9.

Fig. 9 (left) indicated that all simulations showed similar behaviors. Even the coarse mesh with only 450 k elements vaguely represented the roll response of the hull. However, when the last 3 s of the roll decay (Fig. 9 on the right) was closely examined, it was seen that the ship was non-oscillating around the $\phi = 0$ condition and this was physically incorrect. Increasing the number of elements leveled the ship and established the oscillation at around $\phi = 0$ and this result is shown in the same figure.

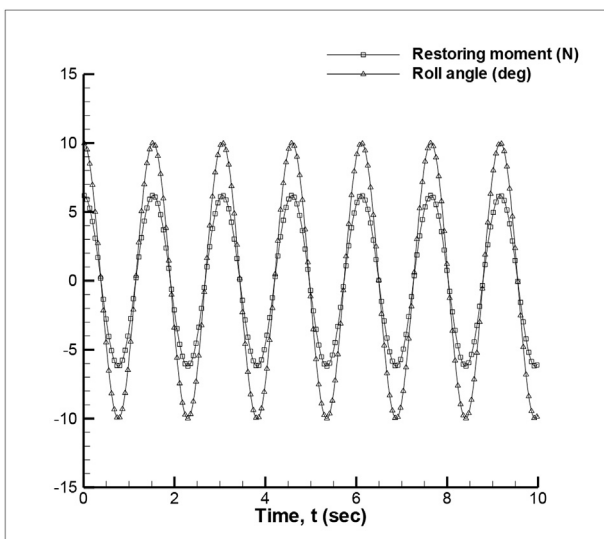


Fig. 10. Variation of the roll angle and the restoring moment with respect to time for the undamped case.

5. Effect of wave and eddy dampings in roll decay

Total roll damping B_T can be expressed in five components (Himeno, 1981):

$$B_T = B_v + B_w + B_e + B_{fs} + B_{bk} \quad (1)$$

In this equation; B_v denotes the viscous damping, B_w the wave damping, B_e the eddy damping, B_{fs} the damping due to forward speed (in other words; lift damping) and B_{bk} the damping due to the existence of the bilge keel. In this study, the bilge keel effect was not a primary source of concern. Therefore, it was not distinguished from the ship but instead, it was considered as a part of the ship. For more information regarding bilge keel effects investigated by RANSE, please refer to (Irvine et al., 2013; Araki et al., 2014; Avalos et al., 2014; Irkal et al., 2014, 2016).

Numerical simulations in this section were for ships with zero forward speed only, and the effects of viscosity were neglected. When these were considered, there were neither B_{fs} nor B_v contributed to total roll damping. Therefore; in this section, the ship roll was only damped due to wave and eddy damping that form in the fluid.

$$B_T = B_w + B_e \quad (2)$$

In this section, the effects of wave damping, and eddy damping were investigated with inviscid numerical flow simulation. The results were supported with the mathematical model. Both methods were used to understand the combined effects of wave and eddy damping in roll decay. To understand the weaknesses of these methods, the numerical and analytical results were assessed by comparison. Stepwise approach was determined as appropriate. The roll decay was mathematically defined starting from the undamped case and including the damping terms on top of the equation of motion.

5.1. The undamped roll equation in roll decay

The undamped roll motion equation is given as:

$$I_{xx} \frac{d^2\phi}{dt^2} = -M_{st} \quad (3)$$

where I_{xx} is the mass moment of inertia of the ship, ϕ is the roll angle and M_{st} is the restoring moment. The restoring moment M_{st} is created by the ship itself due to the existence of the surrounding fluid. The mass moment of inertia can be expressed in terms of the radius of gyration k_ϕ as:

$$I_{xx} = \frac{\Delta}{g} k_\phi^2 \quad (4)$$

The restoring moment of the ship for small values of the roll angle is:

$$M_{st} = \Delta \cdot GM \cdot \phi \quad (5)$$

where GM denotes the metacentric height. Using equations (4) and (5) to substitute into equation (3) and rearranging will bring:

$$\frac{d^2\phi}{dt^2} + \frac{g \cdot GM}{k_\phi^2} \phi = 0 \quad (6)$$

The natural frequency is defined as:

$$\omega_n = \frac{\sqrt{g \cdot GM}}{k_\phi} \quad (7)$$

and substitution of ω_n will return the undamped roll motion equation:

$$\frac{d^2\phi}{dt^2} + \omega_n^2 \phi = 0 \quad (8)$$

Solution of equation (8) for the roll angle is:

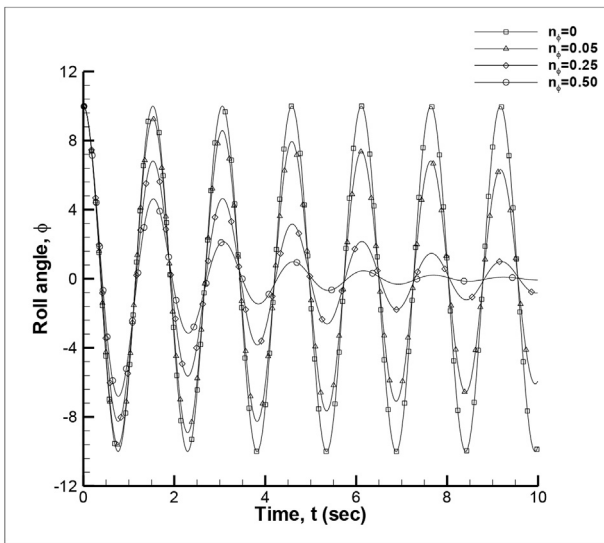


Fig. 11. Roll damping for various n_ϕ .

$$\phi = A \cos(\omega_n t) + B \sin(\omega_n t) \tag{9}$$

Constants A and B are maintained using the initial conditions. For a ship with an initial roll angle ϕ_0 and $d\phi/dt = 0$ at $t = 0$, $A = \phi_0$ and $B = 0$. Therefore, the solution of our roll motion equation becomes:

$$\phi = \phi_0 \cos(\omega_n t) \tag{10}$$

5.2. Roll angle and moment history of DTMB 5512 for the undamped case

The roll angle was determined by equation (10) and the only moment component for the undamped case (which is the restoring moment) was obtained from equation (5). Using the hydrostatic parameters of the DTMB5512 hull for an initial roll angle of $\phi_0 = 10^\circ$, the roll and moment history is given in Fig. 10.

The roll angle and moment would keep oscillating infinitely since there were no outside effects to introduce damping into the roll motion equation. The ship would spend the restoring moment created due to a predetermined initial roll angle and swing back and forth forever in time without any damping.

5.3. The damped roll equation in roll decay

There are some contributions from the fluid that oppose the restoring moment, M_{st} , on the ship which lead to resisted rolling in water. When this additional moment is depicted with M_r , the damped roll equation becomes,

$$I_{xx} \frac{d^2 \phi}{dt^2} = -(M_{st} + M_r) \tag{11}$$

where M_r is the sum of M_w (the moment lost to create waves), M_v (the moment lost due to friction) and M_e (the moment lost to create eddies). It is known that M_v is nonlinear (ITTC 7.5-02-07-04.5, 2011) and in proportion with $(d\phi/dt)^2$ (Bhattacharyya, 1978) and considered to be small compared to other components. Neglecting viscous effects, M_r can be defined as,

$$M_r = M_w + M_e = A_\phi \frac{d\phi}{dt} \tag{12}$$

where A_ϕ is a constant specific to a ship. Rearranging the equation using equation (7) and substituting,

$$2n_\phi = (gA_\phi) / (k_\phi^2 \Delta) \tag{13}$$

a second order linear ordinary differential equation is obtained:

$$\frac{d^2 \phi}{dt^2} + n_\phi \frac{d\phi}{dt} + \omega_n^2 \phi = 0 \tag{14}$$

When this differential equation under roll decay was solved for boundary conditions; $\phi = \phi_0$ and $d\phi/dt = 0$ at $t = 0$, we will obtain the damped roll equation for a ship in roll decay:

$$\phi = e^{-n_\phi t} \phi_0 \left(\cos \omega_{n,d} t + \frac{n_\phi}{\omega_{n,d}} \sin \omega_{n,d} t \right) \tag{15}$$

where $\omega_{n,d}$ is the damped natural roll frequency of the ship and defined as:

$$\omega_{n,d} = \sqrt{\omega_n^2 - n_\phi^2} \tag{16}$$

Equations (15) and (16) define the roll character of the ship under wave damping and eddy damping only.

5.4. Roll history of DTMB 5512 for the damped case

The roll angle history of DTMB 5512 can be obtained using equation (15) for different values of n_ϕ . This value is a measure of damping acting on the ship hull. For an initial roll angle $\phi_0 = 10^\circ$, the ship roll over time is given in Fig. 11 for different n_ϕ .

In Fig. 11, the case $n_\phi = 0$ represents the undamped roll angle history of DTMB 5512 which was given in Fig. 10. This was expected since $n_\phi = 0$, the damped roll angle equation given in (15) is the undamped roll angle equation given in (10). The damped natural frequency of roll given in equation (16) also becomes equal to the undamped natural frequency of roll when n_ϕ is set as 0. It must be noted that the natural frequency of roll seems to be equal for all cases of n_ϕ in Fig. 11. This is an incorrect perception. Based on equation (16), $\omega_{n,d}$ should change as n_ϕ changes; but this variation of n_ϕ reflects as a minor change in the roll period of the hull (due to $\omega_n \gg n_\phi$).

The effects of wave and eddy damping were briefly introduced in this and previous sections using an analytical approach. However, one drawback of this method should be explained further. While calculating these moments, the ship hull form is included in calculations in a limited manner. The effect of the hull form on wave and eddy moments is shrunk to a constant A_ϕ (equation (12)). However, this is a very complex phenomenon. For obtaining applicable results, this effect is linearized. The constant A_ϕ is one of the parameters included in n_ϕ (equation (13)).

However; in the CFD results which were presented in the following sections, the ship hull form and the free water surface were also included. The existence of the hull form and the free surface in calculations significantly changed the roll response of the ship.

5.5. The effect of the free surface and the hull form – wave damping and eddy damping

Existence of a free water surface generates waves as the ship hull makes a roll motion. The wave system generated by the hull is one of the factors that of roll damping. The wave generation is also dependent on the form of the hull. During roll, a ship will create eddies at both sides of the hull. These two factors namely; the surrounding waves and eddies near the hull were investigated in this section to evaluate wave and eddy damping in roll decay. The roll equation in this case should cover the moment to generate waves and eddies. The change in the restoring moment M_{st} with respect to time is given in Fig. 10. The effect of the additional moments M_w and M_e in roll decay were investigated. It was also possible to distinguish the wave damping using the strip method (ITTC 7.5-02-07-04.5, 2011). Yet, in this study, the effects of waves and

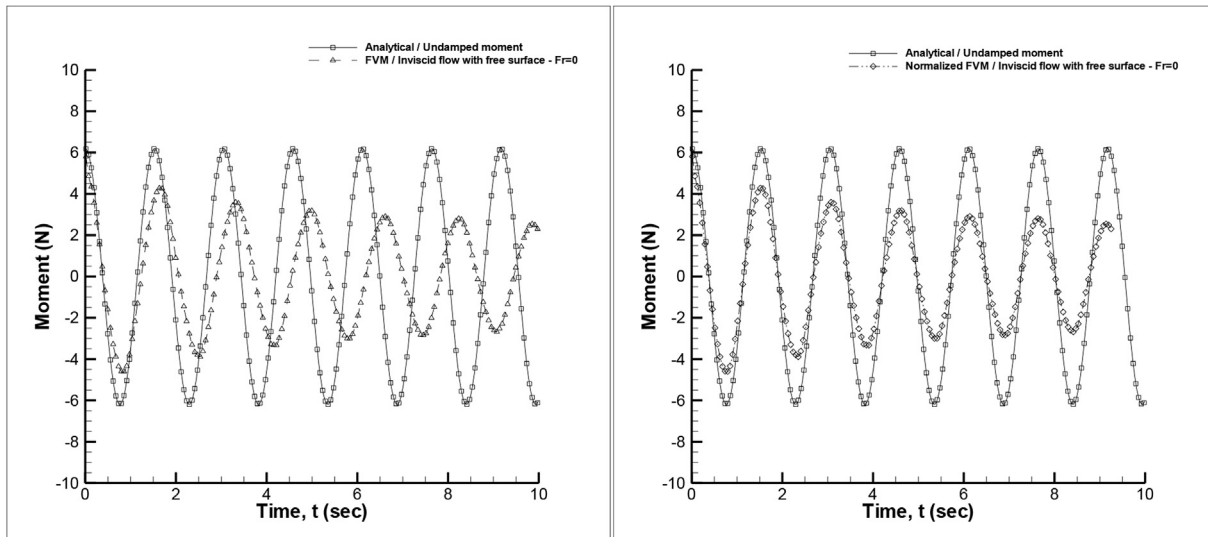


Fig. 12. CFD results of inviscid flow in comparison with analytical method (left). Normalized CFD results vs. analytical method (right).

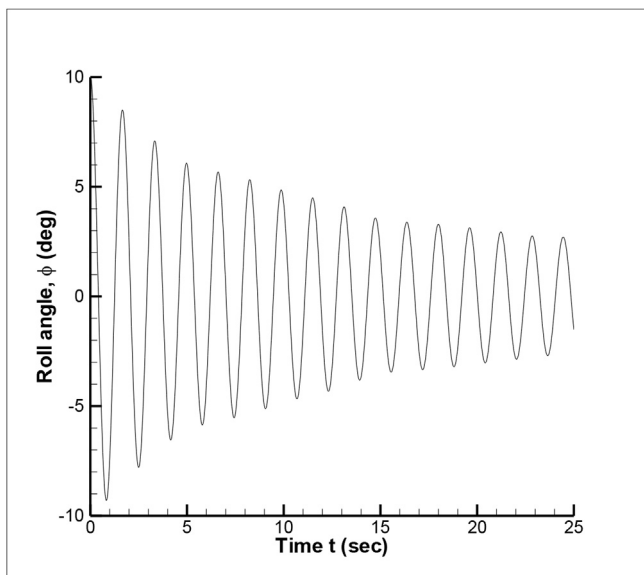


Fig. 13. Roll decay in inviscid flow at $Fr = 0$.

eddies were handled together using RANSE based method only.

These moments that damp the roll motion was obtained by a roll decay CFD simulation in inviscid flow. The simulation included the free water surface to consider the effect of the waves. The total moment calculated by the CFD simulation was subtracted from the restoring moment M_{st} (equation (5)) to obtain the moment t to generate waves and eddies. The ship had zero forward speed so that there was no additional moment created by surge velocity of the ship. The numerical simulation was initiated with an initial roll angle $\phi_0 = 10^\circ$. Total moment ($M_{st} + M_w + M_e$) changes over time are given in Fig. 12 (left).

Fig. 12 (left) shows the change in moment and the difference in period generated by CFD. There was significant and visible decrease in the maximum total moment due to the moment applied to generate the waves and eddies. When periods are considered, the results of the inviscid CFD solution with the free surface at $Fr = 0$ had larger values than the results of the analytical solution. Therefore, it might be commented that the numerical results may be non-compliant with the analytical results. The roll and related restoring moment period of the ship was found as $T = 1.54s$ as stated in (Irvine et al., 2013). However,

the mean period of roll calculated in this study was $T_w = 1.63s$. This is also given in Table 6 and from that table the mean period can be calculated.

When the rolling period was non-compliant with the analytical results, the results obtained for $(M_w + M_e)$ could be misleading. For example, at $t = 9s$ in Fig. 12 on the left-hand side, it is clear that the moment calculated by numerical simulations were outside the phase of the analytical results. If $(M_w + M_e)$ was calculated this way, for the effect of wave and eddy damping, a large value would be obtained. This would be physically incorrect. However, for low values of n_ϕ ; $\omega_{n,d} \cong \omega_n$ for DTMB 5512 (Irvine et al., 2013), the conditions are valid. Therefore, one option was to compact the moment graph as given in Fig. 12(right) so that the period would match the analytical roll period. This way; the phase difference (which might happen because of modeling or numerical errors) between the numerical results and the experiments was eliminated. This process is believed to be more suitable to assess numerical simulations.

Without the interference of viscosity, the ship seems to roll infinitely. Although the amplitude of roll will damp at a slower pace at each period, the amplitude may never reach to zero. The first 25 s of roll decay at an initial roll angle of $\phi_0 = 10^\circ$ is given in Fig. 13. In that Figure, it can be observed that the peak of the ship roll angle is limited around $\phi = 3^\circ$ and has no total damping (see Table 6). The ship would disturb the calm free surface at the beginning of roll decay and transfer some energy to the waves. However, this energy would continuously be transferred between the ship and the free surface. The flow has no component to damp this transfer. In nature, viscosity helps to damp the roll (this topic will be investigated in the following section). It should be once noted that in the numerical simulations in this section, the flow was inviscid. Therefore, roll behavior of the ship was expected to be infinite.

On contrary to inviscid numerical simulation results presented in this section, it was shown in previous sections that if n_ϕ was set to a relatively high value (i.e. $n_\phi = 0.50$ in Fig. 11), infinite rolling was not observed. This is because the mathematical model for damped roll angle equation presented in section 5.4 neglected the energy transfer between the waves and the ship. The numerical simulations allow solving the actual ship in waves and communicating via velocities and accelerations induced on the ship and the free surface. The numerical simulations actually solve for the real fluid-structure interaction problem, whereas the mathematical model only approaches the problem with a reduced order methodology (the moment spent to generate waves and eddies was roughly taken as an order of $d\phi/dt$).

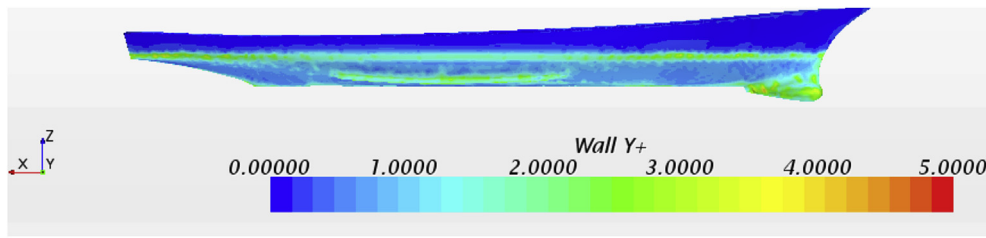


Fig. 14. Wall y^+ distribution along the hull at $Fr = 0$.

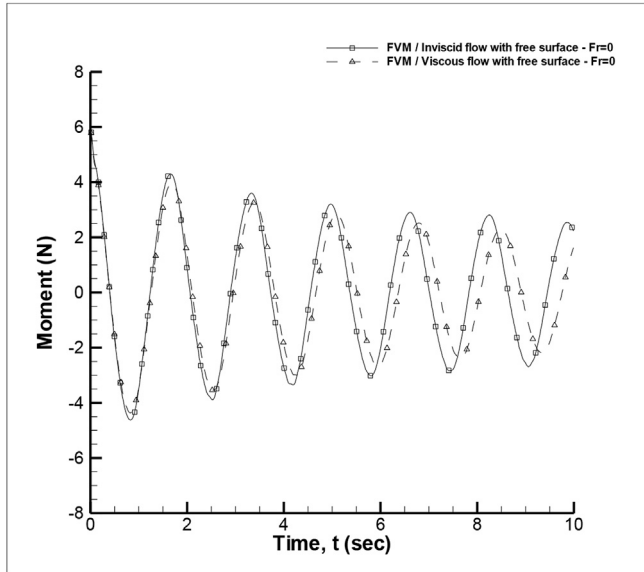


Fig. 15. The effect of viscosity on the total roll moment for $Fr = 0$.

6. Other effects in roll decay: viscosity and forward speed

6.1. The effect of viscosity – viscous damping

With the approach implemented in this study, the different damping sources were discretized first. Later, these sources were superimposed to understand the individual effects. However, they are actually intertwined and have secondary effects on each other. The addition of the viscous damping into the roll motion equation with the free surface would turn the equation into:

$$I_{xx} \frac{d^2 \phi}{dt^2} = -M_{st} - M_w - M_e - M_v \quad (17)$$

In this equation, M_v denotes the moment to overcome the viscosity of the fluid. For the discretization of the viscous damping, a viscous roll decay CFD simulation at $Fr = 0$ was made and compared with the inviscid solution given in the previous section. The initial conditions of the numerical simulations were same as it was previously, except that there was a $k - \epsilon$ turbulence model implemented in the simulations for the viscous and turbulent fluid. To correctly model the turbulent flow around the vessel, necessary gridding should be made along the hull. As it is widely known, this can be achieved by investigating the wall y^+ distribution. Wall y^+ values along the hull at $Fr = 0$ are given in Fig. 14. The moment components M_{st} and $M_w + M_e$ were already known from previous sections. Therefore, the inclusion of M_v was expected to change the moment acting on the hull. The viscous damping effect on the total moment (that includes all the terms in the right-hand side of equation (17)) can be seen from Fig. 15.

Without viscosity, the period of ship roll would have been shorter. Naturally, completely eliminating viscosity on experimental setup is

impossible. However, CFD allows theoretically remove viscosity and solve for inviscid flow. The results given in Fig. 15 were in line with the expectations. Again, there was an increase in the period due to the inclusion of viscosity in the numerical simulations. The period lagged the roll motion and limited the total moment as well since some of the moment was used for the viscosity of the fluid. The shear stress between the molecules consumed some of the energy of the ship. From Fig. 15, although this change was exaggerated in numerical simulations, it might be suggested that viscous damping changed the natural period of roll.

Although the numerical simulations in this study were applied for the model scale ship (including reference experiments are for the model scale), it must be noted that viscous effects tend to decrease with increasing ship size. (ITTC 7.5-03-02-03, 2011) stated that for full ships, the viscosity only accounts for 1–3%. When full scale ship was considered, viscosity will be less influential for increasing Reynolds number.

6.2. The combined effect of viscous, wave and eddy dampings

The analytical solution that was explained in section 5.1 where the results were presented in section 5.2, is only valid when there are no flow disturbances. When the ship hull interacts with the flow, the viscosity, free surface and eddies will be subjected to observable effects. In this context, their influence on roll decay were analytically presented in sections 5.3 and 5.4.

Viscosity, free surface and eddies will consume the moment created by the ship to achieve stability in water. It may be suggested that these constitute the response of the fluid to the roll decay of the hull. Eddies created near the bilge keels during a full period of ship roll is given in Fig. 16. These had effects on the damping of the roll angle and the decrease of the natural frequency of roll. These lagged the motion of the vessel to create extra damping that lead increased periods of motion and diminished roll angles.

6.3. The effect of forward speed

Roll decay is usually evaluated at zero forward speed but when in surge, there will be an additional moment term acting on the ship hull. This is called the forward speed moment, M_{fs} . When forward speed moment is included, the roll equation becomes:

$$I_{xx} \frac{d^2 \phi}{dt^2} = -M_{st} - M_w - M_e - M_v - M_{fs} \quad (18)$$

The forward speed moment will change the roll decay behavior of the vessel. The effects may be seen by applying surge velocity on the ship in numerical simulations. The effects of M_{st} , M_w , M_e and M_v were previously investigated. In this section, the initial conditions were same. However, roll decay was analyzed with a forward ship speed at $Fr = 0.41$. The forward speed effect on the total moment can be seen from Fig. 17.

In terms of diminishing total roll moment; free surface, viscosity and forward speed are similar. On the other hand, the forward speed decreased the roll period of the vessel unlike the wave and viscous effects. Waves and viscosity slowed down the roll motion but increased Fr . Reduced roll period with increased forward speed is also visible in Fig. 18.

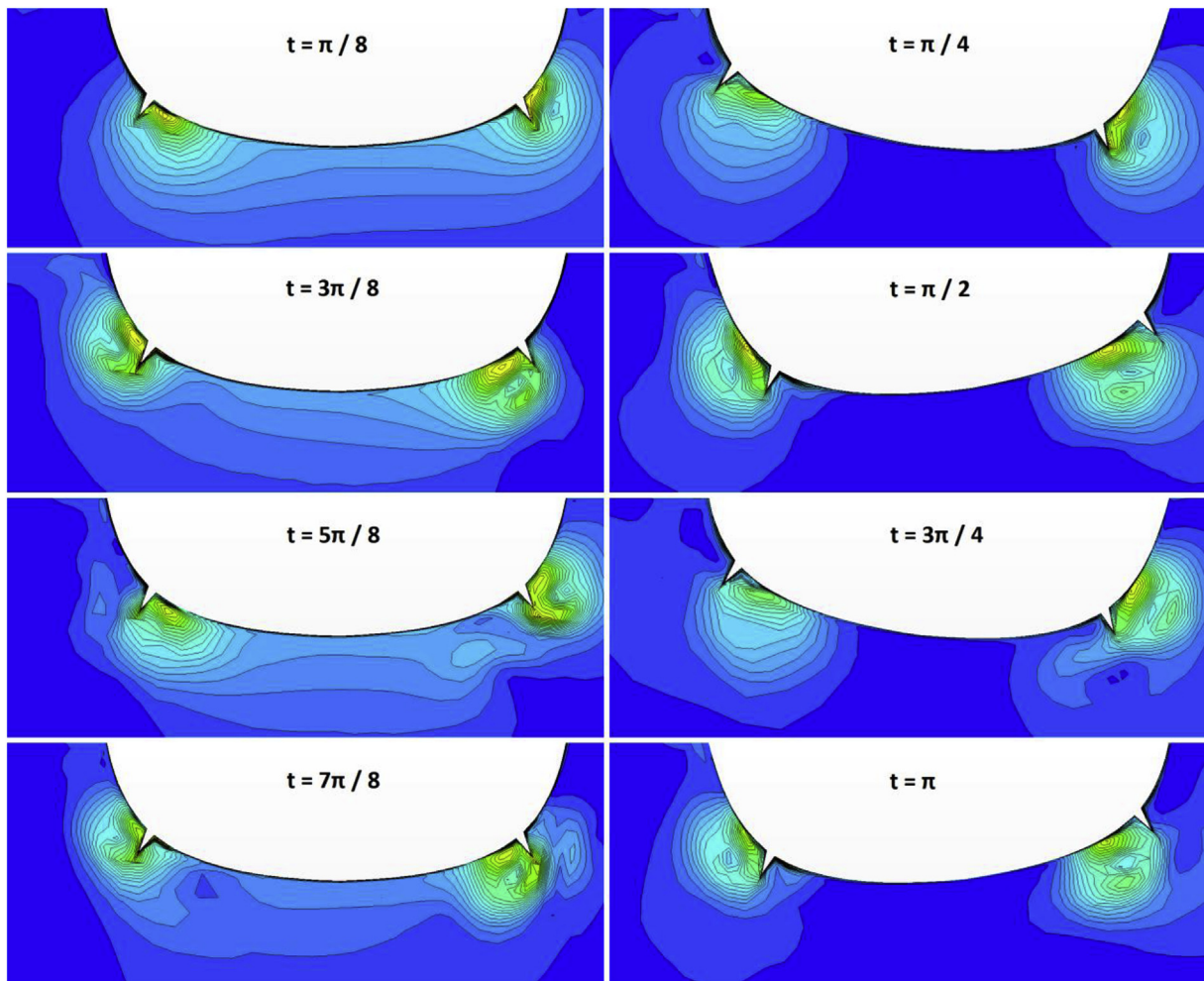


Fig. 16. Velocity contours reveal formation of eddies in the vicinity of the hull during a full period of roll.

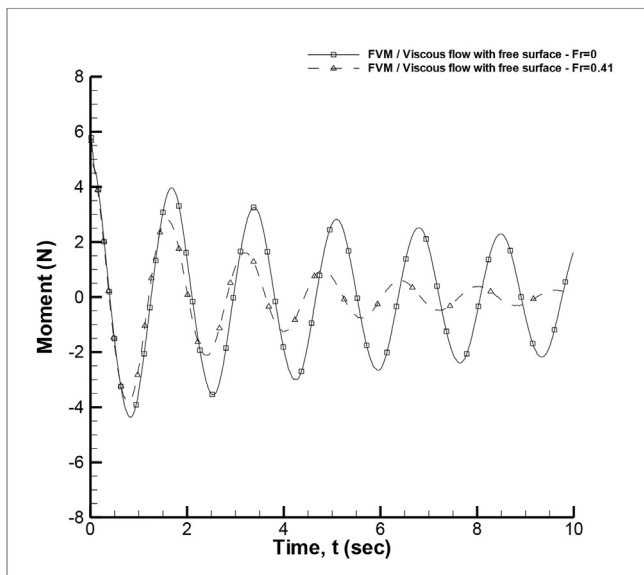


Fig. 17. The effect of forward speed on the total roll moment.

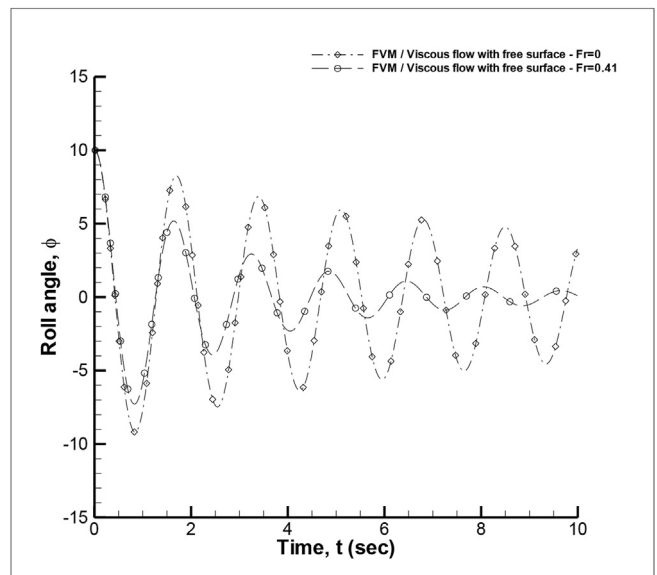


Fig. 18. The effect of forward speed on roll history.

Previous studies reported that roll damping increases as the Froude number increases (Haddara and Zhang, 1994). The experiments of (Irvine et al., 2013) also indicated the same fact. Yet, (Taylan, 2004)

suggested that there is a limit where roll amplitudes are no longer affected by the forward speed. Although the range of $0 < Fr < 0.41$ was partially investigated, the numerical results of the present study

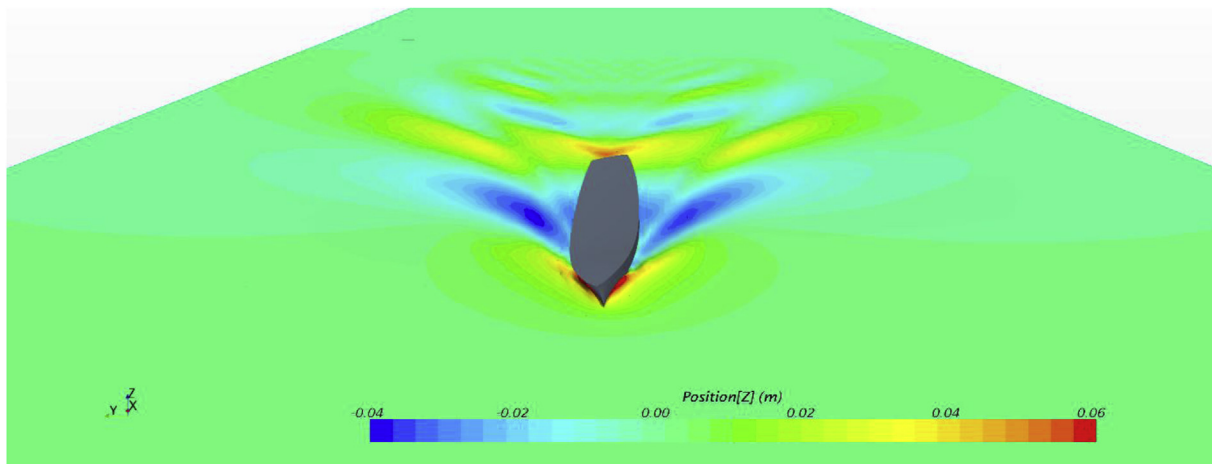


Fig. 19. Formation of waves during roll motion.

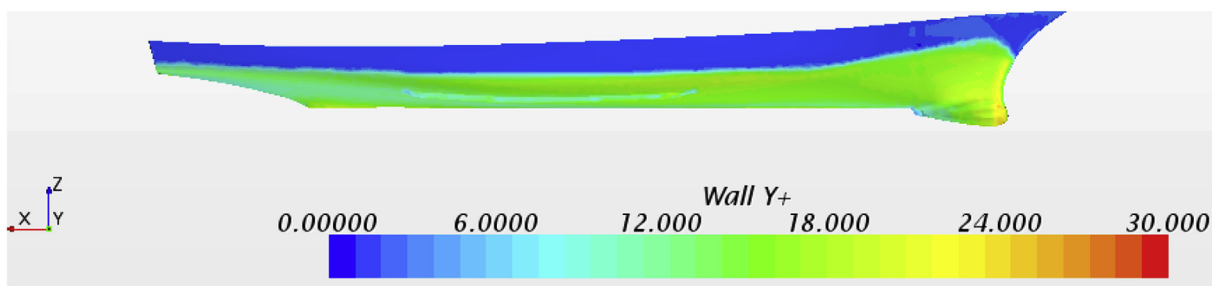


Fig. 20. Wall y^+ distribution along the hull at $Fr = 0.41$.

also suggest that increasing the forward speed helps ship roll damping. Fr number where DTMB 5512 is unresponsive to roll damping was not determined in this study. However, it should be noted here that Taylan (2004) suggested that there is a critical speed where roll damping of the ship is stable although speed is increased. The author reported the critical speed for a $L = 50m$ ship at $Fr = 0.23$. Yet, the author also stated that this value tends to change for ship types. Roll angle histories of the hull with zero forward speed and $Fr = 0.41$ are compared in Fig. 18.

(Colbourne, 1983) stated that wave damping is the major contributor of higher roll damping due to increased Froude number. Although this study has no solid evidence on this subject, this hypothesis is plausible when the hull energy loss occurs at each half cycle while moving forward and creating waves at higher speed. The free surface elevations created during the roll motion of the hull is given in Fig. 19.

Increased forward velocity will also increase the wall y^+ distribution along the hull. This is crucial and must be evaluated in detail as coarse grid around the adverse pressure zones of the hull may lead to inadequate perception regarding the flow in the fluid domain. Although the $k - \epsilon$ turbulence model can relatively handle flows with higher y^+ values, extremely high values of this parameter are undesired. However, even with a high forward speed at $Fr = 0.41$, wall y^+ values are within acceptable range. This is given in Fig. 20.

7. Conclusions

The main purpose of this study was to present the RANSE based CFD capability of the coupled and uncoupled ship roll problem in calm water and presenting numerical results for other numerical studies. Related literature still has few studies regarding computational ship roll results. The aim of this study was to partially fill this gap in the literature.

Another gap in the literature for the numerical roll damping estimation was identified as validation procedures. In this study, a two-step approach with the roll histories of the ship was found appropriate. In this study, the numerical results were validated with the experiments by the curve of decay (which constitutes vertical compliance with the experiments) and natural roll period (which constitutes horizontal compliance with the experiments).

Using this valuable tool and with the aid of mathematical models; various parameters affecting the ship roll such as free surface, eddies, viscosity and forward speed were investigated on DTMB 5512 ship. Related weaknesses of both approaches were explained. It was found out that RANSE based CFD is promising at calculating the curve of decay. However, it still has problems to accurately calculate the roll period. On the other hand, roll period of a ship is roughly known from the geometric properties of the hull. It is possible to normalize results and obtain high compliance with the experiments.

RANSE based CFD is an advanced tool to assess the contributions of different components defined by Ikeda. Due to nonlinear theoretical background; CFD can be used to elaborate the research on ship roll damping. This could be adopted when Ikeda's method is linearized and is unable to correctly predict roll response at certain cases. However, when all RANSE based CFD results in related literature were considered, it is believed that more advanced turbulence models are needed to approximate the motion in more accurate manner. Experiments should still constitute the core for ship roll predictions, but computational studies can open the way for different methods to better understand the components of roll damping.

There are some studies in the literature implementing overset mesh and obtaining better results than the other grid systems. Future studies can use overset mesh to solve the ship roll problem and reveal the advantages of this specific grid implementation.

References

- Acanfora, M., De Luca, F., 2016. An experimental investigation into the influence of the damage openings on ship response. *Appl. Ocean Res.* 58, 62–70.
- Araki, M., Ohashi, K., Hirata, N., 2014. An analysis of bilge keel effects using RANS with overset grids method. In: *The 14th ISSW*, pp. 216–228. Kuala Lumpur.
- Avalos, G.O.G., et al., 2014. Roll damping decay of a FPSO with bilge keel. *Ocean Eng.* 87, 97–110.
- Begovic, E., Day, A.H., Incecik, A., 2017a. An experimental study of hull girder loads on an intact and damaged naval ship. *Ocean Eng.* 133, 47–65.
- Begovic, E., et al., 2017b. Applicability of CFD methods for roll damping determination of intact and damaged ship. In: *High Performance Scientific Computing Using Distributed Infrastructures*, pp. 343–359.
- Bhattacharyya, Rameswar, 1978. *Dynamics of Marine Vehicles*. John Wiley & Sons Inc.
- Chen, H.C., Liu, T., 2002. Time-domain simulation of large-amplitude ship roll motions by a chimera RANS method. *Int. J. Offshore Polar Eng.* 12 (3), 206–212.
- Colbourne, D.B., 1983. *The Effect of Forward Speed on Ship Roll Damping*. MSc. Thesis. MIT.
- Falzarano, J., Somayajula, A., Seah, R., 2015. An overview of the prediction methods for roll damping of ships. *Ocean Sci. Eng.* 5 (2), 55–76.
- Gao, Z., Gao, Q., Vassalos, D., 2011. Numerical study of damaged ship motion in waves. In: *The 12th ISSW*, pp. 257–261 (Washington, USA).
- Gao, Q., Vassalos, D., 2011. Numerical study of the roll decay of intact and damaged ships. In: *The 12th ISSW*, pp. 277–282 (Washington, USA).
- Gu, M., et al., 2016. Validation of CFD simulation for ship roll damping using one pure car carrier and one standard model. In: *The 15th ISSW*, pp. 165–172 (Stockholm, Sweden).
- Haddara, M.R., Zhang, S., 1994. Effect of forward speed on the roll damping of three small fishing vessels. *J. Offshore Mech. Arctic Eng.* 116 (2), 102.
- Himeno, Y., 1981. *Prediction of Ship Roll Damping – a State of the Art*. University of Michigan.
- Ikeda, Y., Himeno, Y., Tanaka, N., 1978. *A Prediction Method for Ship Roll Damping*. Report of the Department of Naval Architecture. University of Osaka Prefecture. Report no. 00405.
- Irkal, M.A.R., Nallayarasu, S., Bhattacharyya, S.K., 2014. *Experimental and CFD Simulation of Roll Motion of Ship with Bilge Keel*. MARHY 2014, Chennai, India.
- Irkal, M.A.R., Nallayarasu, S., Bhattacharyya, S.K., 2016. CFD approach to roll damping of ship with bilge keel with experimental validation. *Appl. Ocean Res.* 55, 1–17.
- Irvine, Martin, Longo, Joseph, Stern, F., 2013. Forward speed calm water roll decay for surface combatant 5415: global and local flow measurements. *J. Ship Res.* 57 (4), 202–219.
- ITTC 7.5-03-02-03, 2011. *Recommended Procedures and Guidelines: Practical Guidelines for Ship CFD*.
- ITTC 7.5-02-07-04.5, 2011. *Recommended Procedures and Guidelines: Numerical Estimation of Roll Damping*.
- Jaouen, F., Koop, A., Vaz, G., 2011. *Predicting Roll Added Mass and Damping of a Ship Hull Section Using CFD*. OMAE2011, Rotterdam.
- Lee, S., et al., 2012. Preliminary tests of a damaged ship for CFD validation. *International Journal of Naval Architecture and Ocean Engineering* 4, 172–181.
- Lee, S., et al., 2016. Experimental study on the six degree-of-freedom motions of a damaged ship floating in regular waves. *IEEE J. Ocean. Eng.* 41 (1), 40–49.
- Sadat-Hosseini, H., Kim, D.H., Carrica, P.M., Stern, F., 2016. URANS simulations for a flooded ship in calm water and regular beam waves. *Ocean Eng.* 120, 318–330.
- Sukas, O.F., Kinaci, O.K., Cakici, F., Gokce, M.K., 2017. Hydrodynamic assessment of planing hulls using overset grids. *Appl. Ocean Res.* 65, 35–46.
- Taylan, M., 2004. Effect of forward speed on ship rolling and stability. *Math. Comput. Appl.* 9 (2), 133–145.
- Wasserman, S., Feder, D.F., Abdel-Maksoud, M., 2016. Estimation of ship roll damping – a comparison of the decay and the harmonic excited roll motion technique for a post panamax container ship. *Ocean Eng.* 120, 371–382.
- Yildiz, B., et al., 2016. URANS prediction of roll damping for a ship hull section at shallow draft. *J. Mar. Sci. Technol.* 21 (1), 48–56.